Lab on a Chip

PAPER

View Article Online
View Journal | View Issue

Cite this: *Lab Chip*, 2017, **17**, 1060

Dielectrowetting manipulation for digital microfluidics: creating, transporting, splitting, and merging of droplets†

Hongyao Geng,[a] Jian Feng,‡[b] Lisa Marie Stabryla[c] and Sung Kwon Cho*[a]

Received 3rd January 2017,
Accepted 10th February 2017

DOI: 10.1039/c7lc00006e

rsc.li/loc

Generating, splitting, transporting, and merging droplets are fundamental and critical unit operations for digital (droplet-based) microfluidics. State-of-the-art digital microfluidics performs such operations commonly using electrowetting-on-dielectric (EWOD) in the typical configuration of two parallel channel plates. This paper presents such operations using dielectrowetting (derived from liquid dielectrophoresis), not EWOD, with an array of interdigitated electrodes. The major and unique feature is that the present droplet manipulations are effective for conductive (water with/without surfactant) and non-conductive (propylene carbonate) fluids. An equally important aspect is that the manipulations are performed in an open space without the covering top plate. This behavior is attributed to the intrinsic nature of dielectrowetting to generate stronger wetting forces than EWOD (with the ability to achieve complete wetting with contact angle = 0° to form a thin film). Using dielectrowetting, micro-droplets of various volumes are created from a large droplet and transported. Splitting a single droplet as well as multiple droplets and merging them are also achieved, even when the droplets are smaller than the electrode pads. The above splitting, transport, and merging operations are effective for propylene carbonate as well as DI water with/without surfactant, though the creating operation is proven only for propylene carbonate at this moment. All the above manipulations are successfully carried out on a single plate, which not only simplifies the structure and operation procedure, but could also eliminate the restriction to the volume of fluid handled.

Introduction

Microfluidic control is essential and critical for lab-on-a-chip (LOC) or micro total analysis system (μTAS) applications. There have been two main streams dealing with controlling microfluids: one is channel-based continuous microfluidics and the other is droplet-based digital microfluidics. Although channel-based microfluidics has been massively and widely exploited[1,2] and promoted for a great number of applications,[3,4] there still exist several disadvantages in such systems: the functionality is not generally reconfigurable after design and fabrication, limiting more flexible applications; the small dimensions of microchannels often generate many fluid mechanics issues such as high pressure drop and clogging; mechanical components, such as pumps, tubes[5] (including connectors) and valves,[6–8] are required for most cases tremendously increasing the complexity of the systems. In contrast, digital microfluidics which is operated by droplets, complementarily solves many of the above issues encountered in the channel-based continuous counterpart.

Among many methods, electrowetting-on-dielectric (EWOD) is one of the most popular and commonly used principles in digital microfluidics.[9,10] The general configuration of EWOD digital microfluidics is that aqueous liquid droplets are sandwiched between two plates with arrayed electrodes on one of the plates and a grounding electrode on the other.[11] The arrayed electrodes are covered by a dielectric and hydrophobic layer while the grounding electrode is covered by a thin hydrophobic layer. These layers prevent direct contact between the droplet and electrodes and maintain high initial contact angles. Upon applying an electric potential between the droplet liquid and electrode, free charges screen the solid–liquid interface, generating an electrohydrodynamic force at the three-phase contact line in the droplet, which changes the contact angle and thus actuates the droplet. Using this driving scheme, aqueous droplets can be driven following programmed paths. In particular, creating, cutting, transport, and merging of droplets constitute essential droplet unit operations, which equivalently

[a] *Department of Mechanical Engineering and Materials Science, University of Pittsburgh, PA 15261, USA. E-mail: hog6@pitt.edu, skcho@pitt.edu*
[b] *Department of Mechanical Engineering and Materials Science, University of Pittsburgh, PA 15261, USA. E-mail: fengxiaojian1983@gmail.com*
[c] *Department of Civil and Environmental Engineering, University of Pittsburgh, PA 15261, USA. E-mail: lms162@pitt.edu*

† Electronic supplementary information (ESI) available. See DOI: 10.1039/c7lc00006e

‡ Currently with Second Sight Medical Products, Inc.

correspond to dispensing, controlling the volume, pumping, and mixing operations in the channel-based continuous counterpart. Cho *et al.*[12] extensively studied and developed these four operations in EWOD where droplets were confined between two parallel plates with a gap. Later, similar droplet actuations and operations were achieved in the two-plate configuration but using liquid dielectrophoresis (L-DEP).[13–18] The L-DEP effect has been widely applied to microfluidics,[19–21] optics,[22–26] diagnostics,[27] microfabrication,[28–31] *etc.* Non-uniform electric fields induce dipoles in liquid that result in a L-DEP force (body force) towards higher field intensity.[32] In this case, the non-uniform electric fields were generated by *solid* shaped electrodes on the plates. In addition, more efforts have been made to investigate the characteristics of L-DEP[33–36] and its distinction from electrowetting.[37] In particular, McHale *et al.*[38,39] introduced a new design of *interdigitated* electrodes on a single plate that generated fringe electric fields. Since the size and spacing of the electrodes are much smaller than those in the two-plate electrode designs, extremely strong electric fields are generated, eventually leading to the superspreading of droplets (zero-degree contact angle). That is, the effect of liquid dielectrophoresis is highly localized to the solid–liquid interface.[38] They coined this phenomenon "dielectrowetting" in analogy to electrowetting. Brown *et al.*[40–43] investigated the underlying physics and applications. However, their droplet actuation was limited to spreading of a single sessile droplet. To date, the development of the four fundamental droplet operations using dielectrowetting has not been made, to the best of the authors' knowledge.

The present paper deals with developing and establishing the four droplet operations (creating, transporting, splitting, and merging of droplets) using *dielectrowetting* as detailed in the following sections. Compared to electrowetting, the present actuation method provides additional advantages: 1) it can easily actuate conductive as well as non-conductive liquids and 2) all required interdigitated electrodes can be installed on a single plate, which means that this system does not necessarily require the top plate (cover), allowing for the handling of a much wider range of liquid volumes with easily accessible and simplified structures.

Theoretical background

The present work applies dielectrowetting for droplet manipulations. Dielectrowetting generates L-DEP forces strong enough to overcome the resistance against droplet movements. Suppose a sessile droplet is placed on the interdigitated finger electrodes (Fig. 1), the working mechanism can be explained by the Korteweg–Helmholtz equation for body force density:[32]

$$\bar{f}^{e} = \rho_{f}\bar{E} - \frac{1}{2}E^{2}\nabla\varepsilon + \nabla\left(\frac{1}{2}E^{2}\rho\frac{\partial\varepsilon}{\partial\rho}\right) \quad (1)$$

where ρ_f and ρ are the free charge density and mass density for fluids, respectively, E is the electric field intensity, and ε is the permittivity of fluids. The first term on the right-hand side denotes the force generated by free charges, which is not considerable for dielectric liquid (ρ_f = 0), the second term represents the L-DEP force, and the last term for electrostriction can be neglected due to incompressibility of liquids. At the interface of liquid and air, the L-DEP force[29,32] is deduced to:

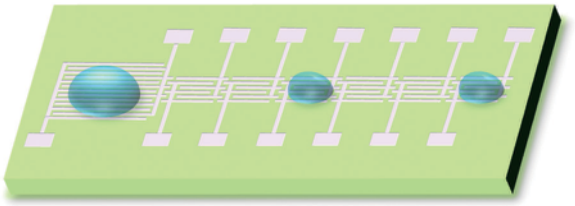

Fig. 1 Schematic of the experimental device: the large interdigitated electrode pad is for a reservoir on which a large droplet sits and from which small droplets are generated. During the experiment, the large droplet stays in the reservoir, while the small daughter droplets are actuated by the six small interdigitated electrode pads. Each electrode pad is activated when an AC voltage is applied between the corresponding signal and ground terminals. To facilitate the continuous motion between two neighbouring pads, interlocking patterns intervene between them (the number of fingers in each electrode is reduced for clarity, and the drawing is not to scale).

$$P_{\text{L-DEP}} = \frac{1}{2}E^{2}\left(\varepsilon - \varepsilon_{0}\right) \quad (2)$$

where ε_0 is the permittivity of air. The stronger electric field and larger permittivity of liquids lead to the larger L-DEP force. Since the fringing electric field in the liquid decays exponentially as the distance increases from the solid–liquid interface, the L-DEP force is largest at the three-phase contact line and decreases rapidly along the liquid–air interface. As a result, the force is confined in the vicinity of the contact line, which is similar to that in EWOD to some extent.[38,44] Meanwhile, the L-DEP force is in the same direction as the interdigitated finger electrodes, giving rise to the anisotropy of contact angle change. That is, the droplet is elongated along the interdigitated electrodes, while the locations and contact angles of the two lateral sides change slightly when the applied voltage remains low. When the voltage is high enough, the strongly generated L-DEP force causes complete wetting of the droplet, which is very difficult for EWOD.

Experimental

Device design and fabrication

The testing device is designed and fabricated as shown in Fig. 1. On a glass substrate, one large electrode set (5 × 5 mm) and six small sets (2 × 2 mm) are arranged in line. The large set serves as a reservoir for the droplet generation, while the smaller digital electrode sets are used for droplet manipulations. Each electrode set consists of two interdigitated finger electrodes, one for signal and the other for

ground. Both the finger width and spacing are 50 μm. A non-uniform electric field is generated between the fingers and pulls the three-phase contact lines along the electrode fingers. Initially, a large droplet is placed on the reservoir, from which small droplets are created. During experiments, the reservoir droplet stays on the reservoir electrode set while the small droplets are generated, split, transported, and merged by the digital small electrode sets. In order to make droplets transiting smoothly between adjacent electrode sets, interlocking electrode fingers (150 μm long and 50 μm wide with identical spacing) are adopted.

The soda lime glass wafer for the substrate was purchased from University Wafer Inc., USA. The electrodes were patterned by standard photolithography. 5 nm Cr and 200 nm Ag layers were deposited by E-beam evaporation, followed by the lift-off process. To avoid any electrochemical reaction between the fluids and the electrodes, a 2 μm thick Parylene C layer was deposited using a chemical vapor deposition (CVD) system (PDS 2010, Specialty Coating Systems). To increase the initial contact angles of the droplets, the surface was treated with Teflon-AF (DuPont, USA) by dip coating and drying on a hotplate (55 °C, 10 min). Before this dip coating, the Teflon-AF solution was diluted with Perfluoro-compound FC-40 (Sigma-Aldrich, USA) solvent to reach a 1% volume concentration.

Experimental setup

In this experiment, alternating current (AC) voltages were supplied to drive the droplets, which allow for deeper penetration of electric fields into the liquids than DC voltage. A function generator (33220A, Agilent) generated a sinusoidal signal, which was amplified by an amplifier (PZD 700, Trek) and transmitted to the circuit. An oscilloscope (199C, Fluke) measured the output, up to several hundred volts, during the experiment. Note that the voltages in this paper denote root-mean-square values. The real-time videos were recorded using a charge-coupled device (CCD) camera (CV S3200, JAI) paired with a microscope. The contact angles were measured by the Contact Angle plug-in in ImageJ software.

The testing fluid was propylene carbonate (Sigma-Aldrich, USA), a common, nontoxic solvent with low volatility (boiling point: 242 °C) and viscosity (0.0025 kg m^{-1} s^{-1}). The surface tension of propylene carbonate is 42 mN m^{-1}. As shown in eqn (2), the large relative permittivity of propylene carbonate ($\varepsilon = 65\varepsilon_0$) increases the L-DEP force. To broaden the application scope of the current dielectric operations, DI (deionized) water with and without surfactant (TWEEN®20, Sigma-Aldrich) was also tested. The surfactant was added to DI water to obtain a 1% (vol/vol) solution and mixed thoroughly to reduce the surface tension of the DI water.

Results and discussion

Droplet spreading

In the experiment, the L-DEP force is desired to be as large as possible. The force is sensitive to the frequency of voltage applied to propylene carbonate as shown in Fig. 2. The contact angle change ($\Delta\theta$) is a good indicator of the L-DEP force. The contact angle at 0 V is 87.6°. At a fixed voltage (175 V), as the frequency increases from 1 kHz to 10 kHz, $\Delta\theta$ increases from 16.2° to 31.0°. In the range of 20 kHz to 100 kHz, $\Delta\theta$ decreases to 14.0° gradually. The optimal frequency occurs at 20 kHz as it induces the greatest contact angle change ($\Delta\theta$ = 32.7°), meaning that the largest L-DEP force is exerted on the droplet to cause spreading. Based on these results, 20 kHz was selected as the frequency for subsequent experiments of droplet manipulations using propylene carbonate.

To see how the magnitude of voltage influences the L-DEP force, and accordingly changes the contact angle, a set of experiments were carried out by changing the voltage. Fig. 3 shows that with increasing voltage, the contact angle decreases from 87.6° (0 V) to 0° (236 V). The relationship between the contact angle change and the voltage can be predicted by the model:[39]

$$\cos\theta(V) = \cos\theta_0 + (1-\cos\theta_0)\left(\frac{V}{V_{Th}}\right)^2 \quad (3)$$

where θ_0 is the contact angle at V = 0 V and V_{Th} is the threshold voltage where the contact angle becomes 0°, *i.e.*, complete wetting. The insets of Fig. 3 show that the profile of the droplet deforms from a half circle, to a circular segment, and to a nearly flat shape at 0 V, 180 V and 236 V, respectively. As the voltage is further elevated, the flat film of the droplet becomes thinner due to the spreading of the droplet across the interdigitated fingers to increase the contact area. This phenomenon is also portrayed in Fig. 4 (movie clip, Movie S1† is available). A droplet (~1.5 μL) is placed at the center of the reservoir, after which the voltages of 180 V, 220 V, 240 V, 280

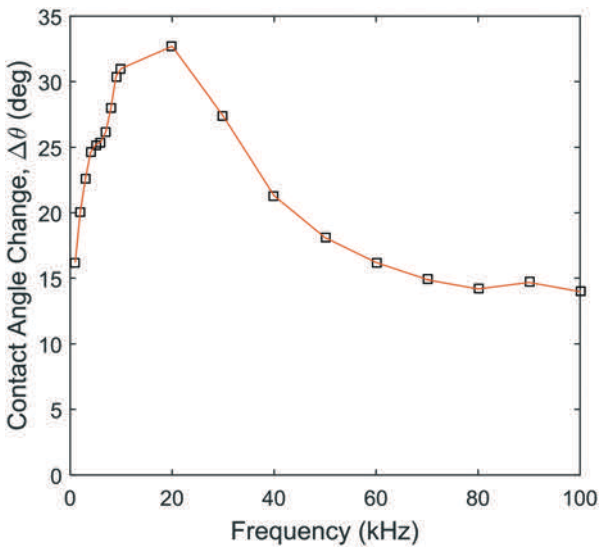

Fig. 2 The effect of frequency on contact angle change of propylene carbonate. The contact angle at 0 V is 87.6°. The maximum change (32.7°) occurs at 20 kHz. The magnitude of voltage is set at 175 V.

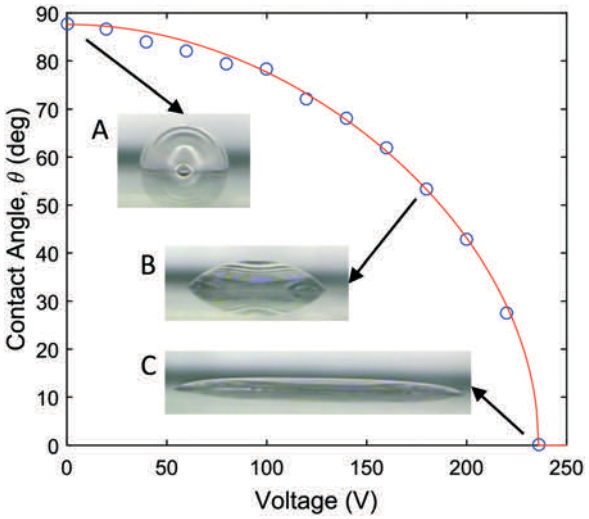

Fig. 3 The effect of voltage on contact angle of propylene carbonate. The solid line from eqn (1) fits the data points well. The inserts show the side views of the droplet at (A) 0 V, (B) 180 V and (C) 236 V. Complete wetting is achieved at 236 V, where the top surface is flat, rather than curved. The frequency of voltages is 20 kHz.

V, 320 V and 360 V are applied. In Fig. 4(b) and (c), dielectrowetting elongates the droplet along the finger electrodes, while no change occurs in the perpendicular direction. Liquid is laterally bounded by the electrode edges and longitudinally pulled along the electrodes, as reported.[38] The contact angle decreases in the longitudinal view, while it remains nearly constant in the transverse view. When the voltage increases to 240 V, as shown in Fig. 4(d), complete wetting occurs. The droplet spreads longitudinally to the left and right boundaries of the electrode pad and transversely crosses the fingers. The top surface of the droplet is flat and the contact angle is 0° when the voltage exceeds 236 V. Fig. 4(e)–(g) show that the spreading is further enhanced as the voltage is increased. The stronger DEP force broadens the contact area and makes the droplet thinner. Finally, in Fig. 4(h), the droplet returns to the hemispherical shape after turning off the power, indicating the reversibility of dielectrowetting. Compared to EWOD using conductive liquids, dielectrowetting with dielectric liquids can stand up to much higher voltages of high frequency. The dielectric droplet has a wider range of contact angle changes, even reaching complete wetting, which is almost impossible for EWOD because of contact angle saturation. The strong DEP force causes the dielectric droplet to deform dramatically.

To further investigate the spreading behavior of dielectric fluids, experiments combining the reservoir and digital electrode pads were conducted. Fig. 5(A) depicts the practicability of the device for droplet spreading. A large droplet (~65 μL) nearly covers the whole reservoir initially. All the electrode pads are connected to the same voltage source. The frequency is maintained at 20 kHz while the voltage is increased to spread the droplet to the small electrode pads. Fig. 5(A2)–(A6) show that the droplet can reach digital electrode pads no. 1, 2, 3, 4, and 6. The fluid exactly fills the footprints of the digital pads when spreading, except for no. 1. Fig. 5(B) summarizes the no. of electrode pads up to which the liquid front can arrive as a function of the voltage. At least 160 V is required for the droplet to spread to pad no. 1. When the voltage exceeds 353 V, the droplet can cover the entire area of the electrodes. Increasing the voltage elevates the L-DEP force to drive the liquid front to a farther distance. Interestingly, reaching and staying on pad 5 was not observed for the liquid front in this experiment. In fact, the voltage tolerance for each electrode pad is not constant. The interlocking patterns between two pads help to reduce the energy barriers at the boundaries and then facilitate the transition. When the voltage is high enough, the droplet can easily cross the boundaries of the digital electrode pads.

Droplet generation

Droplet generation is a fundamental operation for digital microfluidic manipulations. Given an excessive volume of

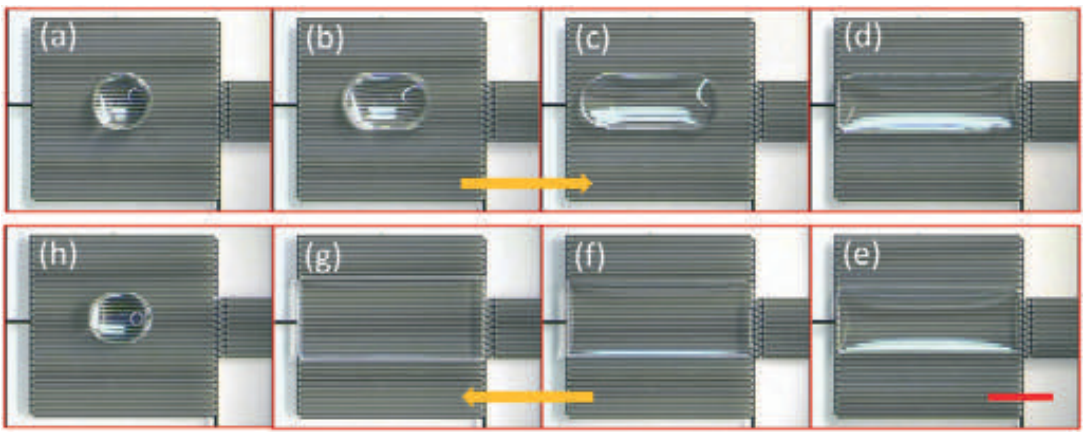

Fig. 4 Top views of a droplet (~1.5 μL) spreading by dielectrowetting at different voltages: (a)–(d) 0 V, 180 V, 220 V, and 240 V, (e)–(h) 280 V, 320 V, 360 V and back to 0 V. Starting at 240 V, complete wetting is achieved. Yellow arrows indicate the sequences of voltages. The frequency of voltages is 20 kHz. The scale bar is 2 mm. A movie clip (Movie S1†) is available.

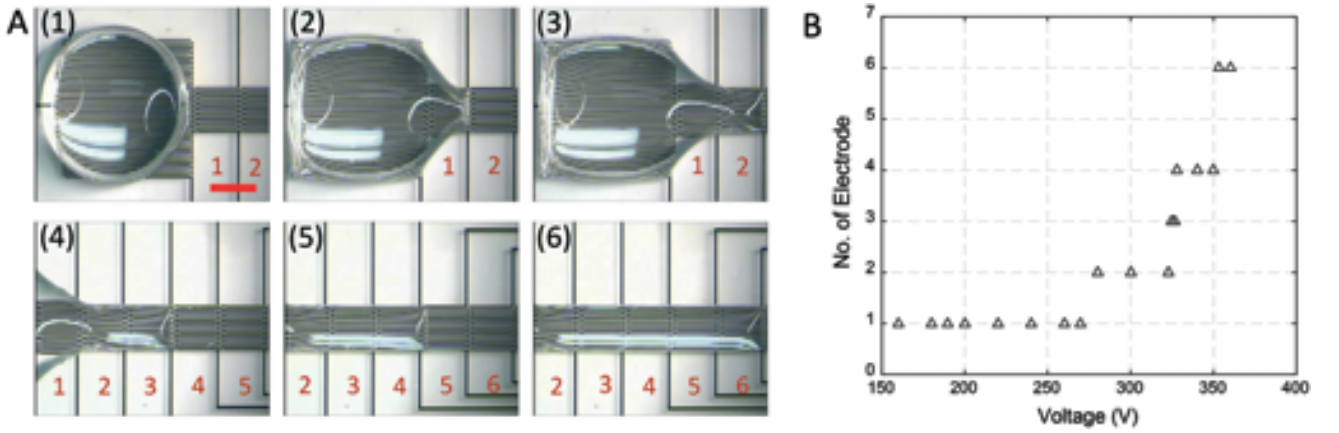

Fig. 5 (A) A large droplet (~65 μL) spreading from the reservoir to digital electrode pads at different voltages (20 kHz): (1) 100 V, stays on the reservoir; (2) 260 V, no. 1 electrode pad; (3) 280 V, no. 2 electrode pad; (4) 325 V, no. 3 electrode pad; (5) 340 V, no. 4 electrode pad; (6) 355 V, no. 6 electrode pad. Both the reservoir and the six digital electrode pads are energized simultaneously. The digital electrode pads are marked with numbers. (B) No. of electrode pad the fluid can reach *versus* voltage applied. The scale bar is 2 mm.

testing fluid sample, it is indispensable to first extract a small metered amount from it for downstream analysis. The present device meets this demand by utilizing dielectrowetting, as shown in Fig. 6. Based on the droplet spreading described above, droplet generation is accomplished at the voltage of 360 V (20 kHz). Fig. 6(A) shows the process in 4 steps (movie clip, Movie S2† is available): firstly, a droplet (~22 μL) as the source, or mother droplet, is dispensed onto the reservoir electrode pad with all pads off; secondly, the large pad and digital pads 1 and 2 are turned on to spread the droplet over the entire activated area; thirdly, digital pad 1 is turned off to neck and cut the droplet; finally, all the pads are turned off to attain a small droplet (~0.9 μL) on digital pad 2. When powering off pad 1, the liquid on it contracts to a neck due to surface tension, and eventually narrows to separate the small daughter droplet from the source droplet. Cutting is achieved almost immediately after digital pad 1 is turned off. In Fig. 6(B), using similar principles, different droplet volumes (~1.6 μL, 2.6 μL and 3.2 μL) are generated by changing the number of activated pads from 2 to 3 and 4. Energizing more pads increases the volume of the created droplet. Meanwhile, after activating 5 pads, two individual droplets are formed because of the hydrodynamic instability of the long liquid thread. For the same reason, tiny satellite droplets are left on digital pad 1 after each trial, as observed in other cutting experiments.[13] All the generated droplets deform rapidly from a thin film to a spherical cap after powering off the electrodes to reach the minimum energy equilibrium. In addition, the created droplets are located in the middle of the activated area.

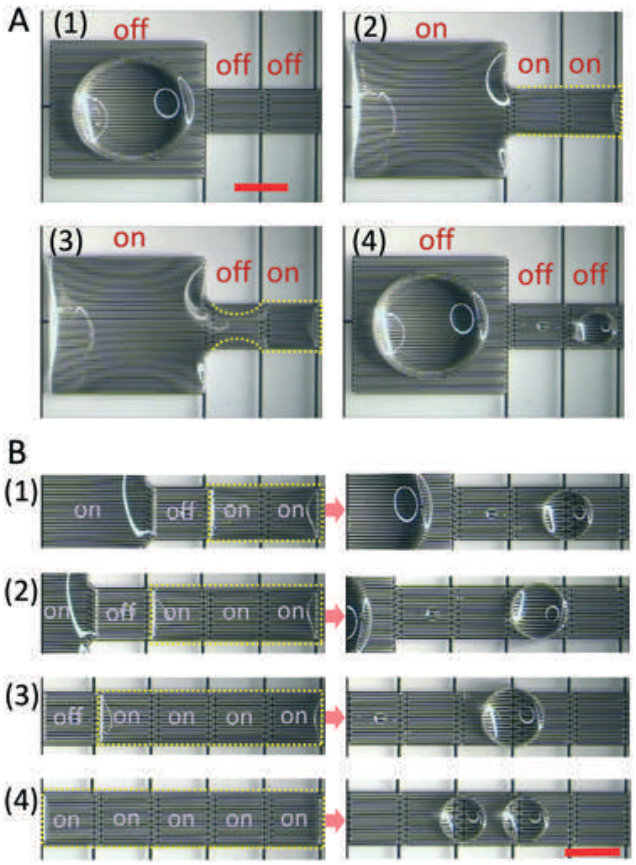

Fig. 6 Droplet generation by dielectrowetting. (A) Four steps of droplet generation: (A1) place a droplet (~22 μL) of propylene carbonate on the reservoir pad; (A2) turn on the three electrode pads (360 V, 20 kHz) to spread the fluid on them; (A3) turn off the middle one to neck and cut the droplet; (A4) turn off all the pads to attain the small droplet (~0.9 μL) on the right. (B) Generating droplets by activating different numbers of electrode pads (after powering off the first one) under the same conditions: (B1) 1.6 μL, 2 pads; (B2) 2.6 μL, 3 pads; (B3) 3.2 μL, 4 pads; (B4) two 1.5 μL droplets, 5 pads. Yellow dashed lines are used to highlight the boundaries of fluid. Scale bars are 2 mm.

Droplet splitting, transport, and merging

More droplet manipulations are achieved on the present digital microfluidics, including splitting, transport, and merging. These operations are carried out under the same conditions: 360 V, 20 kHz. In Fig. 7(a)–(d), a single droplet (~2.3 μL) is

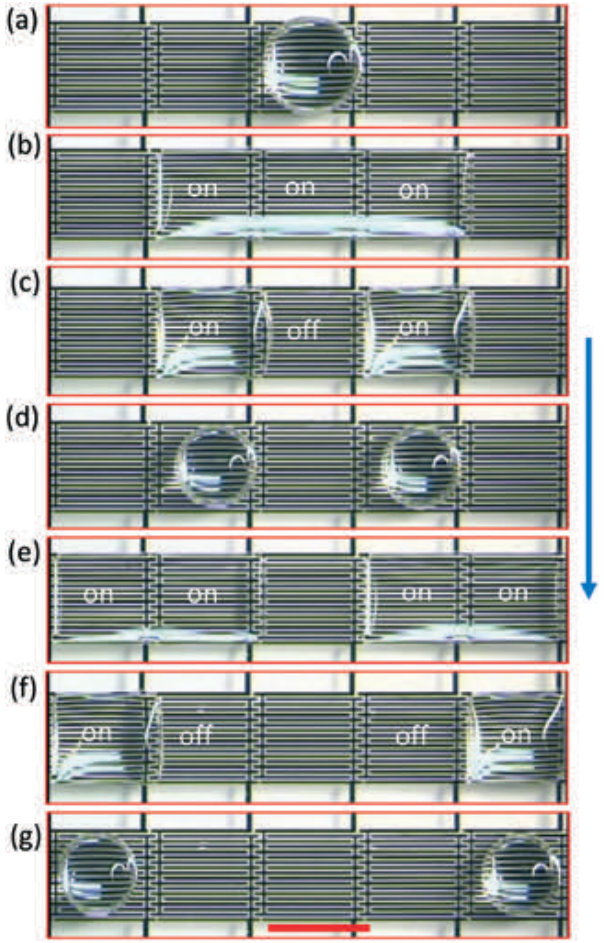

Fig. 7 Droplet splitting and transport (360 V, 20 kHz). (a)–(d) ~2.3 μL droplet split by powering on three pads and then turning off the middle one. (e)–(g) Droplet transported by powering on two pads and then turning off one. The blue arrow shows the time sequence. Scale bar is 2 mm. A movie clip (Movie S3†) is available.

split into two equal smaller droplets by dielectrowetting (movie clip, Movie S3† is available). The mother droplet is stretched into a film when activating the three electrode pads in the middle of the pad array. By powering off the middle pad, two daughter droplets are separated from each other. The remaining electrode pads are turned off to complete the splitting process.

The present splitting procedure is different from that in EWOD. Most importantly, the present splitting does not need the top plate that is in contact with the mother droplet. Namely, splitting can be performed in an open environment while splitting by EWOD works only with pancake-shaped droplets (the mother droplet should be sandwiched between two plates within a critical gap as studied in detail).[12] In addition, for EWOD, the mother droplet should be initially centred on the electrode where no electric potential is applied. Then, it is pulled by the two adjacent electrode pads by changing the contact angles, resulting in neck formation and separation. In this case, the initial position of the mother droplet is critically important to keep the force balance during splitting and to evenly split it. Otherwise, the mother droplet would split into daughter droplets with uneven volumes or simply move to the adjacent electrode pad without splitting. In EWOD, another precondition for successful splitting is that the droplet footprint should be overlapped with some portion of the adjacent electrodes to stretch the mother droplet. Such requirements make the operation delicate and laborious in addition to the complicated fabrication and packaging. More importantly, the two-plate configuration limits the volume of the working fluid due to the small gap between the plates. For the present dielectrowetting device, these issues do not exist when complete wetting is applied to a single mother droplet. The mother droplet footprint does not need to be in contact with the adjacent electrodes. The intermediately formed thin film is spontaneously split by surface tension in an open space after turning off the middle electrode pad.

Similarly, the split droplets can be transported to other positions, as shown in Fig. 7(d)–(g). First, two electrodes are turned on so that the droplet spreads over both (one is the electrode on which the droplet currently sits and the other is the electrode adjacent to where the drop currently sits but where it will move towards). Next, the electrode on which the droplet initially sits is powered off while the adjacent electrode remains activated. The entire volume of the droplet moves to the adjacent electrode. All the electrodes are powered off to complete the droplet transportation.

In EWOD, it is very difficult to split one droplet into more than two new droplets due to the limitation explained above. However, the present dielectrowetting method overcomes this difficulty, as depicted in Fig. 8(a)–(d) (movie clip, Movie S4† is available). One droplet (~3.4 μL) covers the entire area of five electrode pads when activating them at the same time. Multiple splitting is realized by turning off the alternating electrode pads, followed by turning off the remaining pads. The three discrete droplets after splitting can be reunited by powering on five pads and then turning them off, as shown in Fig. 8(e) and (f). This demonstrates the ability to merge several droplets into a single droplet by one-shot activation.

Manipulations for aqueous liquids

In theory, the liquid used for EWOD should be conductive (aqueous) and performs like a dielectric fluid if the applied frequency is high enough.[38,45] This indicates that aqueous liquids can be actuated by the present electrode design. Coplanar electrodes were previously used to actuate aqueous droplets but did not complete the droplet operations (especially droplet splitting in an open environment).[46,47] In this study, in addition to propylene carbonate, the aqueous liquids, *i.e.*, DI water with and without surfactant, were also tested for droplet splitting and transport using the present dielectrowetting system. All experiments in this section are performed at high frequency (55 kHz). Fig. 9 shows the dependence of the contact angle on the voltage applied for the two liquids. The contact angle of DI water drops from 120° (0 V) to 61° (340 V) and then reaches contact angle saturation;

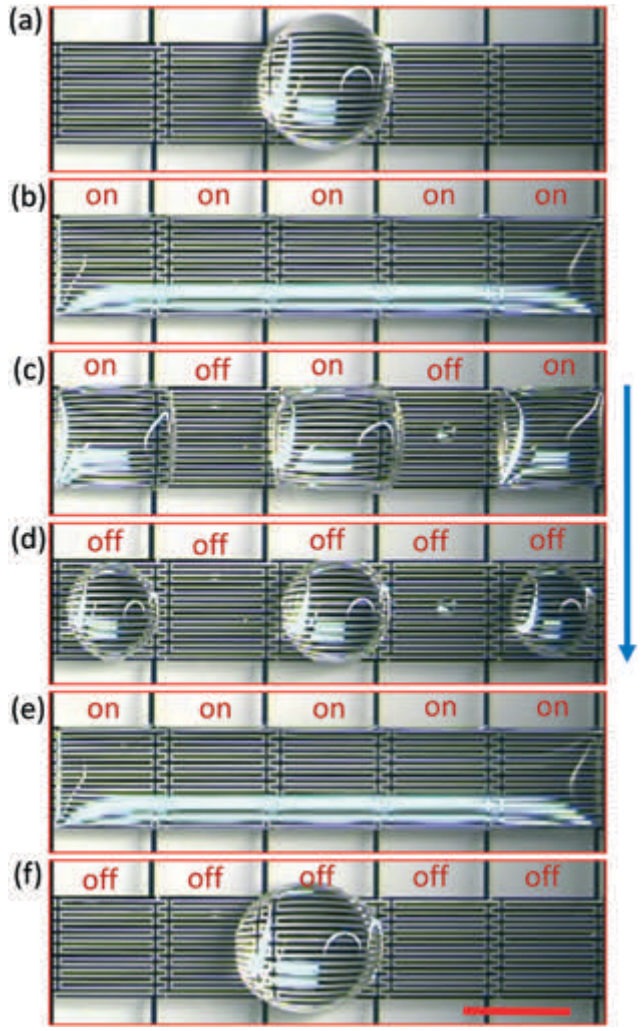

Fig. 8 Multiple splitting and merging (360 V, 20 kHz). (a)–(d) A ~3.4 μL droplet is multi-split by powering on five pads and then turning off the alternating pads. (e) and (f) Three droplets are merged by powering on 5 pads and then turning them off. The blue arrow shows the time sequence. Scale bar is 2 mm. A movie clip (Movie S4†) is available.

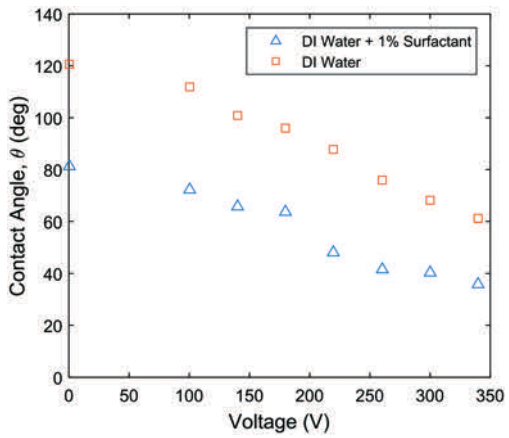

Fig. 9 Contact angle *versus* voltage under the effect of dielectrowetting for DI water with and without surfactant at 55 kHz.

the change is 59°, while the typical change for EWOD is only 40°. Upon addition of 1% surfactant, the contact angle changes from 80° (0 V) to 36° (340 V) with 44° span. The results illustrate that the interdigitated electrode structure is more effective in changing the contact angles of aqueous liquids than solid electrodes in EWOD. Similar to the dielectric liquid case, the contact angles were measured from the longitudinal view of the droplets.

To test whether the L-DEP forces for aqueous liquids are applicable for droplet manipulations in an open space, additional experiments were carried out. Fig. 10 shows the successful transport and splitting of DI water droplets. Adding 1% surfactant produces nearly the same results (images not shown). Since complete wetting is not achieved for aqueous liquids, the mechanisms of moving and cutting are far from the dielectric fluid cases but more similar to those in EWOD. In Fig. 10(A) (Movie S5 in the ESI†), the droplet (~10.8 μL) needs to come into contact with part of the adjacent electrode pad. By applying 340 V to the adjacent pad only, the droplet is transported to the right. Fig. 10(B) (Movie S6 in the ESI†) shows the process of water droplet cutting. The droplet (~7.2 μL) is in contact with two adjacent pads which are then activated by providing voltage (340 V) to them simultaneously. Necking appears in the middle and eventually breaks to produce two small droplets. It is found that increasing the longitudinal length of the electrodes (1.8 × 2.7 mm, with 2 mm spacing in the middle section) facilitates the splitting process by further stretching the droplet. Again note that there is no top plate; the droplet is on a single bottom plate in an open environment. Finally, volume effects on splitting results were investigated, as depicted in Fig. 10(C). At 340 V (55 kHz), the three fluids (propylene carbonate, DI water with and without surfactant) show that threshold volumes exist for splitting. If the volumes exceed the critical values, the droplets are merely elongated and do not split. The threshold volumes are about 4.5 μL, 5.8 μL, and 8.2 μL for DI water with surfactant, propylene carbonate, and DI water without surfactant, respectively. The threshold volumes seem to depend on the initial contact angles, contact angle changes of the fluids, and surface tension but a more in-depth study is required to understand this phenomenon better.

In the current study, all droplet operations are performed in air surroundings. It would be a next step to study that the present droplet operations are applied to droplets immersed in a second liquid (oil), as droplet spreading in the second liquid has been studied previously.[42] Such liquid environments are useful for many digital microfluidic applications. Another interesting topic would be to develop control schemes and systems to manipulate a large number of droplets on a 2-D plane. Like EWOD,[48–54] the present method can be extended to a variety of applications.

Conclusion

This paper describes a novel digital microfluidic circuit based on dielectrowetting. In order to manipulate (create, transport,

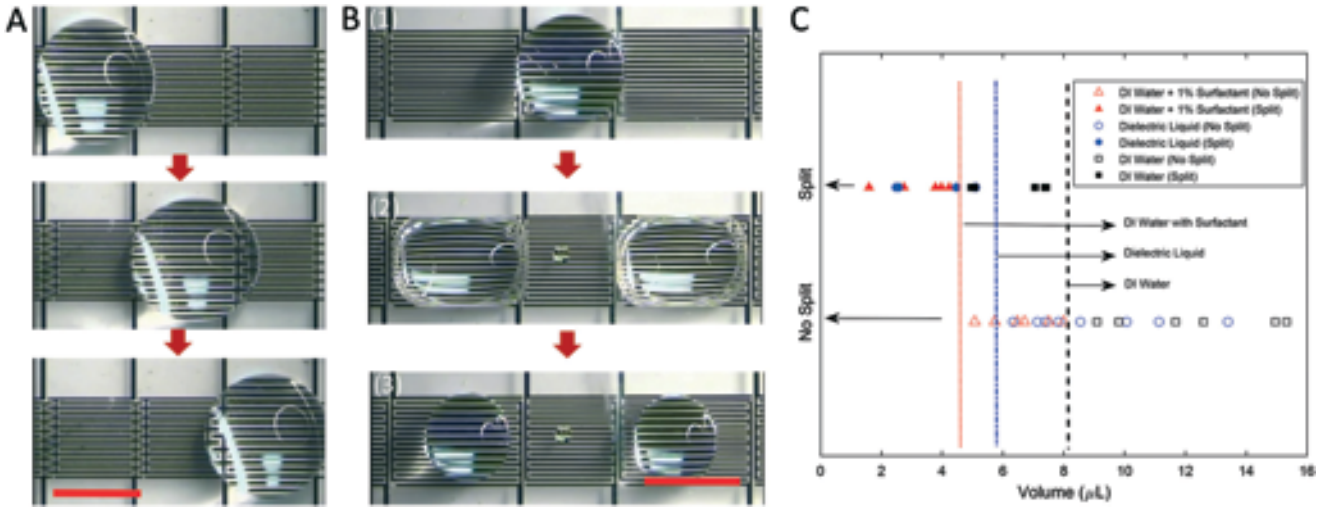

Fig. 10 DI water droplet manipulations by dielectrowetting. (A) Water droplet (~10.8 μL) transporting from left to right. (B) Water droplet (~7.2 μL) splitting sequential procedure. (C) Volume effect on splitting for three liquids: propylene carbonate, DI water with and without surfactant. The three broken lines from left to right show the threshold volumes where splitting occurs for the different liquids. All the manipulations are carried out at 340 V and 55 kHz without a top cover plate. Scale bars are 2 mm. Movie clips (Movies S5 and S6†) are available.

split, and merge) droplets, an individually addressable interdigitated electrode array is designed to generate non-uniform electric fields, which are essential to generate strong L-DEP forces. The L-DEP force is a driving force in dielectrowetting that changes the contact angle even down to 0° at a high voltage. This dielectrowetting actuation is utilized for droplet generation, splitting, transport, and merging. First, the contact angle change, $\Delta\theta$, *versus* voltage and frequency was investigated for dielectric fluid (propylene carbonate). $\Delta\theta$ responds most notably at 20 kHz for propylene carbonate, which is chosen as the operating frequency for the following experiments. The contact angle as a function of voltage is depicted from 87.6° to 0°, and is in good agreement with the given model. Complete wetting occurs when the voltage is elevated to more than 236 V. A single droplet is stretched along the electrodes, without crossing the finger electrode edges. Over the threshold voltage, it starts to spread laterally to the electrodes, resulting in a thin film. The DEP force is large enough to drive the droplet to cross the boundaries between two electrode pads.

Droplet generation with several different volumes is achieved by activating multiple electrodes. The procedure is to pull the liquid from the reservoir to the linear array of digital electrode pads, followed by powering off the first electrode adjacent to the reservoir. The surface tension contracts the droplet to neck and eventually break it into small droplets. Similarly, splitting and transporting are achieved by spreading and turning off the involved electrode pads. Splitting and merging of *multiple* droplets are achieved easily in the present device. To prove the above droplet operations with aqueous (conductive) fluid, DI water with and without surfactant is actuated by the same electrode design. The contact angle of water changes more significantly (from 120° to 61° without surfactant and from 80° to 36° with surfactant), compared to the typical 40° change for water without surfactant in the conventional EWOD. Transporting and splitting for both water fluids are realized. The initial droplet volume effect on splitting is also studied. It should be emphasized that all these droplet operations are achieved in an open environment without the top plate cover.

Acknowledgements

This work is in part supported by the National Science Foundation Grant (NSF ECCS-1637815).

References

1 D. P. Parekh, C. Ladd, L. Panich, K. Moussa and M. D. Dickey, *Lab Chip*, 2016, **16**, 1812–1820.
2 C. Hu, S. Lin, W. B. Li, H. Sun, Y. F. Chen, C. W. Chan, C. H. Leung, D. L. Ma, H. K. Wu and K. N. Ren, *Lab Chip*, 2016, **16**, 3909–3918.
3 E. Dolgin, *Nature*, 2012, **489**, 12–14.
4 Y. P. Chen, W. Gao, C. B. Zhang and Y. J. Zhao, *Lab Chip*, 2016, **16**, 1332–1339.
5 B. G. Chung, K. H. Lee, A. Khademhosseini and S. H. Lee, *Lab Chip*, 2012, **12**, 45–59.
6 O. Cybulski, S. Jakiela and P. Garstecki, *Lab Chip*, 2016, **16**, 2198–2210.
7 H. Gong, A. T. Woolley and G. P. Nordin, *Lab Chip*, 2016, **16**, 2450–2458.
8 J. Hansson, M. Hillmering, T. Haraldsson and W. van der Wijngaart, *Lab Chip*, 2016, **16**, 1439–1446.
9 F. Mugele and J. C. Baret, *J. Phys.: Condens. Matter*, 2005, **17**, 705–774.
10 W. C. Nelson and C. J. Kim, *J. Adhes. Sci. Technol.*, 2012, **26**, 1747–1771.
11 M. G. Pollack, R. B. Fair and A. D. Shenderov, *Appl. Phys. Lett.*, 2000, **77**, 1725–1726.

12 S. K. Cho, H. Moon and C.-J. Kim, *J. Microelectromech. Syst.*, 2003, **12**, 70–80.
13 S. K. Fan, T. H. Hsieh and D. Y. Lin, *Lab Chip*, 2009, **9**, 1236–1242.
14 S. K. Fan, W. J. Chen, T. H. Lin, T. T. Wang and Y. C. Lin, *Lab Chip*, 2009, **9**, 1590–1595.
15 W. Wang and T. Jones, *J. Phys.: Conf. Ser.*, 2011, **301**, 012057.
16 N. Kumari, V. Bahadur and S. V. Garimella, *J. Micromech. Microeng.*, 2008, **18**, 085018.
17 S. K. Fan, P. W. Huang, T. T. Wang and Y. H. Peng, *Lab Chip*, 2008, **8**, 1325–1331.
18 D. Chatterjee, B. Hetayothin, A. R. Wheeler, D. J. King and R. L. Garrell, *Lab Chip*, 2006, **6**, 199–206.
19 P. R. C. Gascoyne, J. V. Vykoukal, J. A. Schwartz, T. J. Anderson, D. M. Vykoukal, K. W. Current, C. McConaghy, F. F. Becker and C. Andrews, *Lab Chip*, 2004, **4**, 299–309.
20 R. H. Temperton and J. S. Sharp, *Langmuir*, 2013, **29**, 4737–4742.
21 S. K. Fan, H. P. Lee, C. C. Chien, Y. W. Lu, Y. Chiu and F. Y. Lin, *Lab Chip*, 2016, **16**, 847–854.
22 C. C. Cheng and J. A. Yeh, *Opt. Express*, 2007, **15**, 7140–7145.
23 Y. C. Wang, Y. C. Tsai and W. P. Shih, *Microelectron. Eng.*, 2011, **88**, 2748–2750.
24 A. Russell, E. Kreit and J. Heikenfeld, *Langmuir*, 2014, **30**, 5357–5362.
25 S. Xu, H. W. Ren and S. T. Wu, *J. Phys. D: Appl. Phys.*, 2013, **46**, 483001.
26 R. Zhao, B. Cumby, A. Russell and J. Heikenfeld, *Appl. Phys. Lett.*, 2013, **103**, 223510.
27 E. O. Adekanmbi and S. K. Srivastava, *Lab Chip*, 2016, **16**, 2148–2167.
28 X. M. Li, Y. C. Ding, J. Y. Shao, H. M. Tian and H. Z. Liu, *Adv. Mater.*, 2012, **24**, 165–169.
29 X. M. Li, J. Y. Shao, H. M. Tian, Y. C. Ding and X. M. Li, *J. Micromech. Microeng.*, 2011, **21**, 065010.
30 H. M. Tian, J. Y. Shao, H. Hu, L. Wang and Y. C. Ding, *RSC Adv.*, 2016, **6**, 77275–77283.
31 H. M. Tian, J. Y. Shao, C. B. Jiang, L. Wang and Y. C. Ding, *Microfluid. Nanofluid.*, 2016, **20**, 118.
32 T. B. Jones, *J. Electrost.*, 2001, **51**, 290–299.
33 Z. Brabcova, G. McHale and G. G. Wells, *Langmuir*, 2016, **32**, 10844–10850.
34 T. B. Jones, J. D. Fowler, Y. S. Chang and C. J. Kim, *Langmuir*, 2003, **19**, 7646–7651.
35 T. B. Jones, R. Gram, K. Kentch and D. R. Harding, *J. Phys. D: Appl. Phys.*, 2009, **42**, 225505.
36 A. C. Russell, W. L. Hsieh, K. C. Chen and J. Heikenfeld, *Langmuir*, 2015, **31**, 637–642.
37 T. B. Jones, *Langmuir*, 2002, **18**, 4437–4443.
38 G. McHale, C. V. Brown, M. I. Newton, G. G. Wells and N. Sampara, *Phys. Rev. Lett.*, 2011, **107**, 186101.
39 G. McHale, C. V. Brown and N. Sampara, *Nat. Commun.*, 2013, **4**, 2619.
40 C. V. Brown, W. Al-Shabib, G. G. Wells, G. McHale and M. I. Newton, *Appl. Phys. Lett.*, 2010, **97**, 242904.
41 C. V. Brown, G. McHale and N. J. Mottram, *J. Appl. Phys.*, 2011, **110**, 024107.
42 C. V. Brown, G. McHale and C. L. Trabi, *Langmuir*, 2015, **31**, 1011–1016.
43 C. V. Brown, G. G. Wells, M. I. Newton and G. McHale, *Nat. Photonics*, 2009, **3**, 403–405.
44 G. McHale, C. V. Brown, M. I. Newton, G. G. Wells and N. Sampara, *Proc. SPIE*, 2012, **8557**, 855703.
45 F. Mugele, A. Klingner, J. Buehrle, D. Steinhauser and S. Herminghaus, *J. Phys.: Condens. Matter*, 2005, **17**, 559–576.
46 A. G. Banpurkar, K. P. Nichols and F. Mugele, *Langmuir*, 2008, **24**, 10549–10551.
47 U.-C. Yi and C.-J. Kim, *J. Micromech. Microeng.*, 2006, **16**, 2053.
48 R. A. Hayes and B. J. Feenstra, *Nature*, 2003, **425**, 383–385.
49 J. Heikenfeld and A. J. Steckl, *Appl. Phys. Lett.*, 2005, **86**, 151121.
50 S. K. Chung, K. Ryu and S. K. Cho, *Appl. Phys. Lett.*, 2009, **95**, 014107.
51 S. Kuiper and B. H. W. Hendriks, *Appl. Phys. Lett.*, 2004, **85**, 1128–1130.
52 B. Berge and J. Peseux, *Eur. Phys. J. E: Soft Matter Biol. Phys.*, 2000, **3**, 159–163.
53 S. K. Chung, Y. Zhao and S. K. Cho, *J. Micromech. Microeng.*, 2008, **18**, 095009.
54 Y. Zhao, S. K. Chung, U. C. Yi and S. K. Cho, *J. Micromech. Microeng.*, 2008, **18**, 025030.

